

Non-uniform plastic deformation of micron scale objects

Christian F. Niordson^{1,*},[†] and John W. Hutchinson²

¹*Department of Mechanical Engineering, Technical University of Denmark, Kgs. Lyngby, DK-2800, Denmark*

²*Division of Engineering and Applied Sciences, Harvard University, Cambridge, MA 02138, U.S.A.*

SUMMARY

Significant increases in apparent flow strength are observed when non-uniform plastic deformation of metals occurs at the scale ranging from roughly one to ten microns. Several basic plane strain problems are analysed numerically in this paper based on a new formulation of strain gradient plasticity. The problems are the tangential and normal loading of a finite rectangular block of material bonded to rigid platens and having traction-free ends, and the normal loading of a half-space by a flat, rigid punch. The solutions illustrate fundamental features of plasticity at the micron scale that are not captured by conventional plasticity theory. These include the role of material length parameters in establishing the size dependence of strength and the elevation of resistance to plastic flow resulting from constraint on plastic flow at boundaries. Details of the finite element method employed in the numerical analysis of the higher order gradient theory will be discussed and related to prior formulations having some of the same features. Copyright © 2003 John Wiley & Sons, Ltd.

KEY WORDS: strain gradient plasticity; size effects; nonlocal mechanics; finite element analysis

1. INTRODUCTION

Recent experiments involving non-uniform plastic deformation of metals at the scale of a micron to tens of microns have revealed a strong size dependence of plastic flow. Small micron-sized objects behave as if their yield strength is as much as two or three times that of larger samples of identical material. The experiments include micro-indentation [1], thin sheet bending [2], wire torsion [3] and thin metal films bonded to elastically deforming substrates [4]. Non-uniform straining is an essential feature in the apparent size-dependence of plastic flow – uniform tension tests display no apparent strengthening with diminishing size on similar sets of wires and sheets used in the torsion or bending tests. It is generally agreed that the strengthening phenomenon is associated with excess dislocations that are generated by gradients of plastic strain. Such dislocations are referred to as geometrically necessary dislocations [3]. Over the size scale ranging from a micron to tens of microns for which most

*Correspondence to: Christian F. Niordson, Department of Mechanical Engineering, Technical University of Denmark, Kgs. Lyngby, DK-2800, Denmark

[†]E-mail: cn@mek.dtu.dk

Received 20 December 2001

Revised 22 April 2002

Accepted 23 April 2002

of the experiments have been conducted and for which there are many potential applications, the number of dislocations is generally so large that a continuum formulation is required to describe deformation. Various efforts are underway to formulate continuum theories of plasticity including those for single crystals [5–7] and phenomenological versions intended to generalize conventional plasticity theory in the simplest meaningful way [3, 8–11]. Potential applications of the theories include structural materials with micron-scale microstructure, MEMS, solder interconnects, and mechanical property determination at the micron scale in films and multilayers.

In the present paper, we employ a recent version of strain gradient plasticity proposed by Fleck and Hutchinson [12] that reformulates an earlier version [8]. While the new version retains the essential physical attributes of the earlier formulation, it is significantly easier to implement within a finite element framework for numerical analysis. The numerical structure of the new version is similar in most respects to the numerical formulation studied in References [13–15] as a means for setting a size scale for shear localizations in plastic and granular materials within the gradient theory of Aifantis [11, 16]. The Fleck–Hutchinson reformulation of strain gradient plasticity used here is a generalization of the classical isotropic hardening theory of plasticity, J_2 flow theory, and it reduces to this theory when the scale of the deformation becomes large relative to the material length parameters. The theory employs a measure of effective plastic strain that depends on both plastic strains and plastic strain gradients. In the most general form, the measure brings in three material length parameters that determine the size dependence of plastic flow. Included as a special case of the theory is a version which employs an effective plastic strain measure with a single material length parameter in a form similar to that proposed by Aifantis *et al.* [11, 16].

The constitutive model is introduced in the next section, emphasizing features that require special attention in numerical implementation. The theory is higher order with higher order stresses, extra boundary conditions, and additional conditions at a boundary separating regions of plastic loading and elastic unloading. The possibility of placing constraints on plastic flow at the boundary with a stiff substrate or platen is discussed and illustrated by way of numerical examples. Three basic plane strain problems have been selected to bring out some of the essential features of plastic flow in micron-sized solids. The first two problems involve the deformation of a rectangular slab bonded to rigid platens on its top and bottom faces and having traction-free ends. The traction-free ends give rise to non-uniform strains, as do the boundaries with the rigid platens if plastic flow is assumed constrained. These two effects are examined as a function of slab aspect ratio for both tangential and normal relative displacements of the platens. The two loading conditions differ in that the normal displacement of the platens produces high hydrostatic tension that combines with the gradient effects to elevate the apparent strength of the slab. The third problem involves indentation by a rigid flat punch into a rectangular elastic-plastic solid on a rigid substrate. The computational results will stress the issue of the choice of the materials length parameters.

2. MATERIAL MODELLING

The material is modelled by a strain gradient generalization of J_2 flow theory proposed by Fleck and Hutchinson (see Reference [12]). In this theory hardening effects due to plastic strain gradients are included through the gradient of the plastic strain rate $\rho_{ijk} = (\dot{\epsilon}_{ij}^p)_{,k} = (m_{ij}\dot{\epsilon}^p)_{,k}$,

where $(\cdot)_{,k}$ denotes the partial derivative with respect to the co-ordinate x_k . Here, $\dot{\varepsilon}^p = \sqrt{\frac{2}{3}\dot{\varepsilon}_{ij}^p\dot{\varepsilon}_{ij}^p}$ is the increment of effective plastic strain, and $m_{ij} = \frac{3}{2}s_{ij}/\sigma_e$ is the direction of the plastic strain increment, where s_{ij} is the stress deviator, and σ_e is the von Mises's effective stress. A new measure of effective plastic strain rate, \dot{E}^p , is defined in terms of three unique, non-negative invariants of ρ_{ijk} which are homogeneous of degree two: I_1 , I_2 , and I_3 (see Reference [12] for details). The positive definite measure has the form

$$\dot{E}^{p^2} = \dot{\varepsilon}^{p^2} + l_1^2 I_1 + l_2^2 I_2 + l_3^2 I_3 \quad (1)$$

where, l_1 , l_2 , and l_3 are material length parameters which set the scale for the strain gradient effects. The effective plastic strain rate can be expressed explicitly in terms of $\dot{\varepsilon}^p$ and $\dot{\varepsilon}_{,i}^p$ in the form:

$$\dot{E}^{p^2} = \dot{\varepsilon}^{p^2} + A_{ij}\dot{\varepsilon}_{,i}^p\dot{\varepsilon}_{,j}^p + B_i\dot{\varepsilon}_{,i}^p\dot{\varepsilon}^p + C\dot{\varepsilon}^{p^2} \quad (2)$$

where the coefficients A_{ij} , B_i and C depend on the material length parameters as well as on m_{ij} and its gradient [12]. These coefficients vanish when the l 's all vanish, or, equivalently, when the scale governing the deformation is large compared to the l 's. The total effective plastic strain is $E^p = \int \dot{E}^p dt$. A one parameter strain gradient theory can be formulated as a special case within the present framework if we take $A_{ij} = l_*^2 \delta_{ij}$, $B_i = 0$, and $C = 0$ such that

$$\dot{E}^{p^2} = \dot{\varepsilon}^{p^2} + l_*^2 \dot{\varepsilon}_{,i}^p \dot{\varepsilon}_{,i}^p \quad (3)$$

This version is closely related to the strain gradient theory of Aifantis [11] as discussed in Reference [12].

The incremental principle of virtual work for the strain gradient plasticity theory can be stated as (see Reference [12])

$$\int_V [\dot{\sigma}_{ij} \delta \varepsilon_{ij}^c + \dot{Q} \delta \dot{\varepsilon}^p + \dot{\tau}_i \delta \dot{\varepsilon}_{,i}^p] dV = \int_S [\dot{T}_i \delta u_i + \dot{i} \delta \dot{\varepsilon}^p] dS \quad (4)$$

where, V and S denotes the volume and the surface of any subset of the entire body, respectively. The stress is denoted σ_{ij} , and $\varepsilon_{ij} = \frac{1}{2}(u_{i,j} + u_{j,i})$ is the strain which is the sum of the elastic strain, ε_{ij}^c , and the plastic strain. The work conjugate to the plastic strain is Q , and τ_i is the higher order stress which is the work conjugate to the gradient of the plastic strain, $\varepsilon_{,i}^p$. In the integrand of the right-hand side of Equation (4), $\dot{T}_i = \dot{\sigma}_{ij} n_j$, and $\dot{i} = \dot{\tau}_i n_i$ denote the traction, and the higher order stress on S , respectively, where n_i is the outward unit normal to S .

The stress measures are related to the strain measures through the incremental relations

$$\dot{\sigma}_{ij} = L_{ijkl}(\dot{\varepsilon}_{kl} - \dot{\varepsilon}^p m_{kl}) \quad (5)$$

$$\dot{Q} = h(E_p) \left(\dot{\varepsilon}^p + \frac{1}{2} B_i \dot{\varepsilon}_{,i}^p + C \dot{\varepsilon}^p \right) \quad (6)$$

$$\dot{\tau}_i = h(E_p) \left(A_{ij} \dot{\varepsilon}_{,j}^p + \frac{1}{2} B_i \dot{\varepsilon}^p \right) \quad (7)$$

where L_{ijkl} is the elastic stiffness tensor for an isotropic solid, and $h(E^p)^{-1} = E_t(E^p)^{-1} - E^{-1}$. Here, E is Young's modulus, and E_t is the tangent modulus, which is evaluated at E^p , and not at ε^p as it would be in conventional J_2 flow theory.

The strong form of the field equations corresponding to the principle of virtual work (4) can be stated as

$$\dot{\sigma}_{ij,j} = 0 \quad (8)$$

$$\dot{Q} = \dot{\sigma}_e + \dot{\tau}_{i,i} \quad (9)$$

together with the boundary conditions

$$\dot{T}_i = \dot{\sigma}_{ij}n_j \quad \text{and} \quad \dot{t} = \dot{\tau}_{i}n_i \quad \text{on } S \quad (10)$$

The yield condition is specified in terms of the generalized effective stress Q , by $Q = Q_y$, where the evolution of Q_y is given by $\dot{Q}_y = h(\dot{\epsilon}^p + \frac{1}{2}B_i\dot{\epsilon}_{i,i}^p + C\dot{\epsilon}^p)$. The initial value of Q_y is equal to the initial yield stress denoted σ_y .

The strain gradient plasticity theory reduces to classical J_2 flow theory when the values of the three material length scales go to zero.

The uniaxial stress–strain curve used in the present paper is defined from the following relation for the tangent modulus in the plastic range

$$E_t(E^p) = \frac{E}{n} \left(\frac{E^p}{\epsilon_0} + 1 \right)^{1/n-1} \quad (11)$$

Here, n is the hardening exponent, and $\epsilon_0 = \sigma_y/E$ is the yield strain in uniaxial tension. The resulting stress–strain curve for pure shear can be seen in Figure 2, where the lower curve shows the conventional pure shear response.

3. NUMERICAL METHOD

The numerical solutions are obtained through a plane strain finite element discretization. The displacement increments, \dot{u}_i , and the strain increments $\dot{\epsilon}_{ij}$, within each element are given from $2k$ nodal displacement increments \dot{D}^n (k is the number of nodes per element with displacement degrees of freedom)

$$\dot{u}_i = \sum_{n=1}^{2k} N_i^n \dot{D}^n \quad \dot{\epsilon}_{ij} = \sum_{n=1}^{2k} E_{ij}^n \dot{D}^n \quad (12)$$

where $N_i^n(x_j)$ are shape functions and $E_{ij}^n = \frac{1}{2}(N_{i,j}^n + N_{j,i}^n)$.

The effective plastic strain increment, and its gradient, are given from l nodal effective plastic strain increments $\dot{\epsilon}_n^p$ (l is the number of nodes per element with degrees of freedom for the effective plastic strain)

$$\dot{\epsilon}^p = \sum_{n=1}^l M^n \dot{\epsilon}_n^p \quad \dot{\epsilon}_{i,i}^p = \sum_{n=1}^l M_{i,i}^n \dot{\epsilon}_n^p \quad (13)$$

where $M^n(x_j)$ are shape functions.

Using these relations in Equation (4) leads to an element matrix for elements in the plastic range of the following form:

$$\begin{bmatrix} \mathbf{K}_e & \mathbf{K}_{ep} \\ \mathbf{K}_{ep}^T & \mathbf{K}_p \end{bmatrix} \begin{bmatrix} \dot{\mathbf{D}} \\ \dot{\boldsymbol{\varepsilon}}^p \end{bmatrix} = \begin{bmatrix} \dot{\mathbf{F}}_1 \\ \dot{\mathbf{F}}_2 \end{bmatrix} \quad (14)$$

where

$$\mathbf{K}_e^{nm} = \int_V [E_{ij}^n L_{ijkl} E_{kl}^m] dV \quad (15)$$

is the elastic stiffness matrix,

$$\mathbf{K}_{ep}^{nm} = - \int_V [E_{ij}^n L_{ijkl} m_{kl} M^m] dV \quad (16)$$

is a matrix of dimension force,

$$\mathbf{K}_p^{nm} = \int_V [m_{ij} L_{ijkl} m_{kl} M^m M^n + h (M^m M^n + A_{ij} M_{,j}^m M_{,i}^n + \frac{1}{2} B_i (M_{,i}^m M^n + M^m M_{,i}^n) + C M^m M^n)] dV \quad (17)$$

is a matrix of dimension energy.

The right-hand side of Equation (14) consists of

$$\dot{\mathbf{F}}_1^n = \int_S \dot{T}_i N_i^n dS \quad (18)$$

which is the conventional external force vector, and

$$\dot{\mathbf{F}}_2^n = \int_S \dot{i} M^n dS \quad (19)$$

which is the higher order traction vector.

The structure of the element matrix is similar to that explored by de Borst *et al.* (see References [13, 14]), within the strain gradient theory of Aifantis [11], in that the plastic strains are treated as free variables and the yield condition is satisfied in a weak sense. However, when it comes to the treatment of boundary conditions several differences from References [13] and [14] will be mentioned in the next section.

The finite element meshes used for solution of the problems considered in the present paper consists of quadrilaterals each subdivided by the diagonals into four triangles. The triangles are linear in $u_{i,}$ and linear in ε^p , which means that $k=l=3$ in the above equations. A three point integration rule is used for the integration of \mathbf{K}_p , in order to avoid spurious modes for the incremental effective plastic strain field [14]. Load integration is carried out using the Forward Euler method.

4. COMPUTATIONAL AND MODELLING DETAILS

The numerical algorithm used to obtain the numerical results is presented in this section. After each increment in external load (or displacement) the stress state is known within each triangular element. For each quadrilateral an average value of the stress tensor is found. Nodal

values of the stress tensor in each corner node of the quadrilaterals are found as the average of the stress tensors in the quadrilaterals connected to a corner node. The stresses are interpolated using standard bilinear shape functions expressed in natural co-ordinates. The gradient of σ_{ij} is evaluated in the centre of each quadrilateral, defined as the origin of the natural co-ordinate system for the quadrilateral. The gradient of m_{ij} is evaluated through

$$m_{ij,k} = \frac{3}{2} \frac{s_{ij,k} \sigma_e - s_{ij} \frac{3}{2} \frac{s_{pq} s_{pq,k}}{\sigma_e}}{\sigma_e^2} \quad (20)$$

and m_{ij} and $m_{ij,k}$ is then used to find A_{ij} , B_i , and C for each quadrilateral. The effective plastic strain, E^p , is updated for each triangle, using m_{ij} , $\dot{\epsilon}^p$, and $\dot{\epsilon}_{,k}^p$ for the triangle and A_{ij} , B_i , and C for the quadrilateral containing the triangle.

The stiffness matrix for the next increment is formed on the basis of E^p , and m_{ij} for each triangular element, and again using A_{ij} , B_i , and C for the quadrilateral containing the triangle.

At an external boundary of a region undergoing plastic deformation both conventional and higher order boundary conditions must be specified. At a free surface where there is no constraint of plastic flow (i.e. dislocations pass through the surface unimpeded), the appropriate higher order condition is that there be no constraint on $\dot{\epsilon}^p$, which is equivalent to the natural boundary condition $\dot{\tau}_i n_i = 0$. At a strongly bonded interface with a stiff solid which does not deform plastically, the higher order boundary condition is $\dot{\epsilon}^p = 0$. This is the appropriate continuum condition that models the fact that dislocations cannot reach the interface and form pile-ups.

Conditions at an internal boundary separating a plastically deforming region from an elastic region in a homogeneous solid require careful consideration. From a physical standpoint, dislocations are free to pass through the current elastic-plastic boundary, and they necessarily do so if the boundary moves as the overall deformation proceeds. This implies that plastic flow should not be constrained at the boundary in a continuum model, i.e. no constraint on $\dot{\epsilon}^p$ in the present formulation. In this sense, the condition is no different from conventional plasticity. However, the consequence of no constraint on $\dot{\epsilon}^p$ in the higher order theory is that $\dot{\tau}_i n_i = 0$ is enforced at the boundary as a natural boundary condition. The traction rate, $\dot{t} = \dot{\tau}_i n_i$, is thereby continuous across the elastic-plastic boundary. An alternative to that just described, that has been discussed [13], takes $\dot{\epsilon}^p = 0$ at the elastic-plastic boundary. In Reference [14], C^1 -continuity of $\dot{\epsilon}^p$ throughout the entire body is used to ensure that both $\dot{\epsilon}^p = 0$ and $\dot{\epsilon}_{,i}^p n_i = 0$ holds at the elastic-plastic boundary. These conditions can be shown to result in $\dot{\tau}_i n_i = 0$ at the boundary by aid of Equation (7). The proper higher order condition modelling plastic flow at the elastic-plastic boundary in a continuum theory for a homogeneous solid remains open for discussion. In this paper, we assume that there is no constraint on plastic flow at an elastic-plastic boundary, as would be the case in conventional continuum plasticity.

Plastic loading is initiated once σ_e becomes larger than the initial yield stress, σ_y . Unloading of an element along the elastic moduli, is started when the solution has found a negative increment of the effective plastic strain within the element in the previous increment.

In the elastic region the free variables for the plastic strain increments are disabled through setting \mathbf{K}_{ep} to zero when forming the element matrix in Equation (14). Furthermore, \mathbf{K}_p is put equal to some small number times the identity matrix (in practical calculations this small number is chosen to be $10^{-8}E$), since this prevents the element matrix for elastic elements to have any significant contribution to the solution of the plastic strain increments of the nodes on the boundary, at the same time as it prevents singularity of the global system matrix.

5. NUMERICAL RESULTS

Numerical investigations of three problems have been carried out. Shear and tension of an elastic-plastic slab between two rigid substrates are studied. Attention is paid to the higher order boundary conditions imposed at the substrates. Finally, indentation by a flat punch of a rectangular solid on a rigid substrate is studied.

5.1. Shear of a finite slab

In this section results are presented on the shear under plane strain conditions of a slab of height $2H$ and width $2L$ occupying the region: $-L \leq x_1 \leq L$ and $-H \leq x_2 \leq H$ (see Figure 1). The top and bottom edges along $x_2 = \pm H$ are bonded to rigid platens that are displaced horizontally according to $u_1 = U$ on $x_2 = H$ and $u_1 = -U$ on $x_2 = -H$ with $u_2 = 0$. The ends of the slab along $x_1 = \pm L$ are traction free. The material in all the examples to be presented in this paper has $\varepsilon_0 = \sigma_y/E = 0.01$, Poisson's ratio, $\nu = 0.3$, and stress hardening exponent, $n = 5$. Gradients in this problem arise from two sources: (i) the traction free ends and (ii) any constraint on plastic flow at the rigid platens. The x_1 -independent solution for the infinite long slab ($L \rightarrow \infty$) according to conventional theory has no gradients of strain in the x_2 direction. Consider first the infinitely long slab, which was discussed by Fleck and Hutchinson [12]. Assuming no constraint on plastic flow at the platens, the conventional solution for the infinite slab is also the solution for the strain gradient plasticity version of the problem. This is an example for which strain gradients do not 'naturally' occur in the conventional approach. If plastic flow is constrained at the platens such that $\dot{\varepsilon}^p = 0$ at $x_2 = \pm H$, gradients are introduced and the conventional theory no longer applies. For this problem the three length parameters combine in the solution into a single length parameter. Moreover, for this example the one-parameter version of the theory can be brought into coincidence with the multi-parameter version if $l_* = \sqrt{\frac{4}{5} l_1^2 + l_2^2 + \frac{6}{5} l_3^2}$ [12]. For both constrained and unconstrained cases, the work

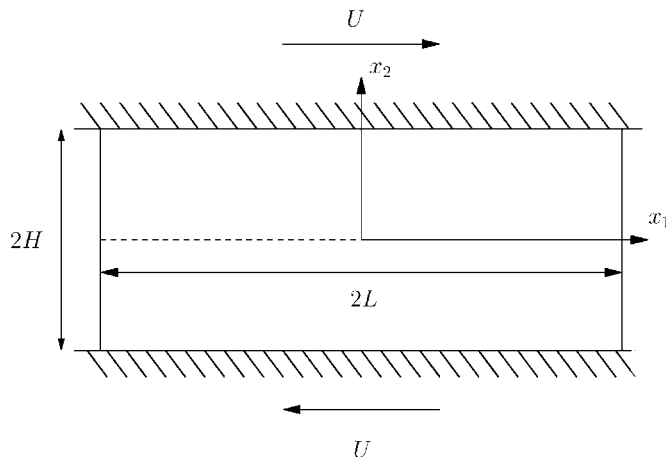


Figure 1. A slab of material between rigid platens is analysed under shear deformation. The elastic-plastic solid occupies the region $-L \leq x_1 \leq L$ and $-H \leq x_2 \leq H$, and the platens are displaced the distance $2U$ relative to each other in the direction of the x_1 -axis.

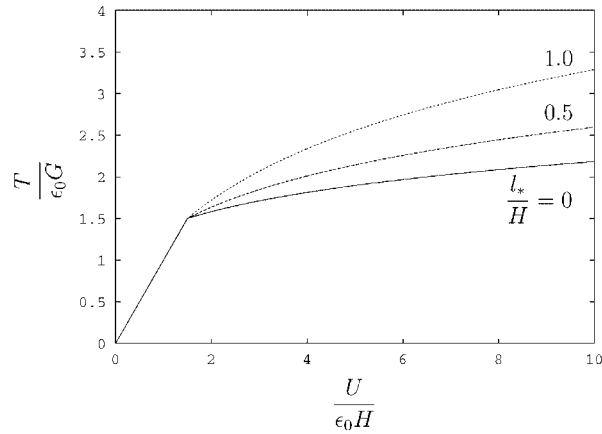


Figure 2. Shear responses for an infinite slab for a conventional material, and for two gradient dependent materials with full constraint on plastic flow at the platens.

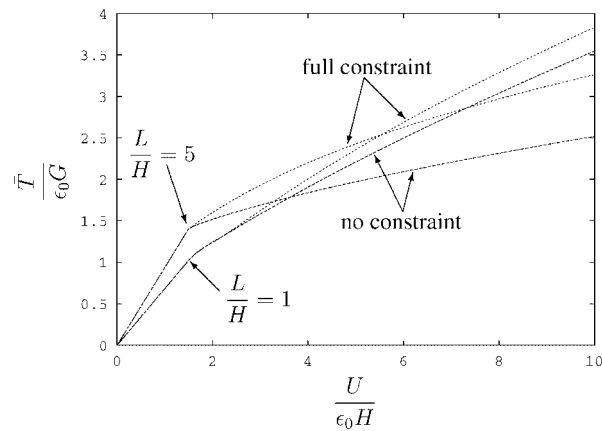


Figure 3. Shear responses for gradient dependent slabs of aspect ratios of 1 and 5. One set of curves show results with full constraint on plastic flow at the platens, while the other set of curves show results with no constraint on plastic flow at the platens. The material length scales are defined by $l_1/H = l_2/H = l_3/H = \frac{1}{2}$.

increment per unit area on the top and bottom faces is $T dU$ where $T = \sigma_{12}$. Curves of the shear traction, T , at the top and bottom of the slab as a function of the overall shear strain, U/H , are presented in Figure 2 for the limit $l_* = 0$ (the conventional result) and for two values of l_* , both with zero plastic strain enforced at the platens.

The effect of the traction free ends in the finite width slabs according to the strain gradient theory is seen in Figure 3 where overall shearing curves are presented as the average shear traction, \bar{T} , as a function of U/H for two slab aspect ratios. All the curves have been computed for the multi-parameter version of the theory with $l_1/H = l_2/H = l_3/H = \frac{1}{2}$. Included in this

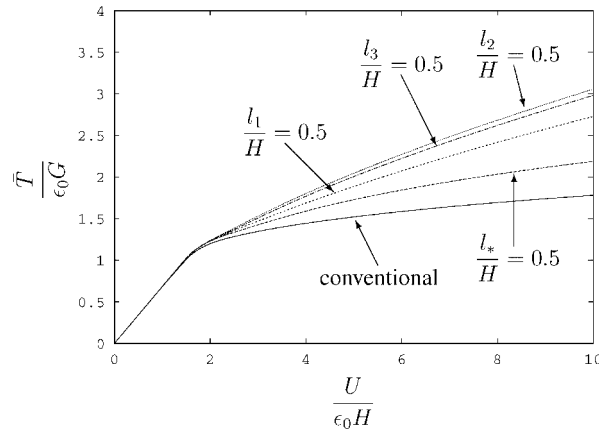


Figure 4. Shear responses for a slab of aspect ratio $L/H = 1$ with full constraint on plastic flow at the platens. For each of the upper 4 curves one of the length parameter is put equal to $H/2$, with all other length parameters put equal to zero. The lower curve shows the response for a conventional solid.

figure are results for both constrained ($\dot{\epsilon}^p = 0$) and unconstrained ($\dot{\epsilon} = 0$) plastic flow at the platens. (Plastic flow at the ends is unconstrained.) The influence of the finite aspect ratio shows up even in the elastic range where higher order effects are entirely absent. In the plastic range, the finite aspect of the slab induces gradients of strain in the conventional solution, and thus there is an influence on the apparent hardening even when the plastic flow is unconstrained at the platens. Indeed, for the square slab ($L/H = 1$), the effect of constraining the plastic flow at the platens provides a relatively small additional hardening. For the higher aspect ratio ($L/H = 5$), constraint on plastic flow produces most of the elevation in hardening, as would be expected from the limit for the infinite slab. Now, the case where plastic flow is unconstrained at the platens is not very different from the conventional solution (not shown).

Further results for shear of the square slab ($L/H = 1$) for different choices for the material length parameters are presented in Figure 4. Several interesting features are revealed in this plot. The conventional solution falls below the corresponding curve for the infinite slab in Figure 2. This is due to the fact that the shear stress vanishes on the ends reducing stiffness in both the elastic and plastic ranges. It can also be seen that the single parameter version of the gradient theory ($l_*/H = \frac{1}{2}$) falls below the curve for the corresponding infinite slab in Figure 2. By contrast, the multi-parameter versions all predict higher hardening than the corresponding results for an infinite slab of the same material. The difference in behaviour predicted for the multi-parameter and the single parameter versions arises from the measures of the gradients of plastic strain involved in the two versions. In the single parameter version, only the gradient of the effective plastic strain, $\dot{\epsilon}_{i,j}^p$, is used in the measure, while in the multi-parameter version, all components, $\dot{\epsilon}_{ij,k}^p$, enter the measure. At the free edges, it can be shown that $\dot{\epsilon}_{i,1}^p = 0$ for the single parameter version ($\dot{\epsilon}_{i,1}^p n_i = 0$ is a consequence of the natural boundary condition), and thus there is no gradient contribution in the vicinity of the edges. There is a non-zero gradient contribution at the edges according to the multi-parameter versions.

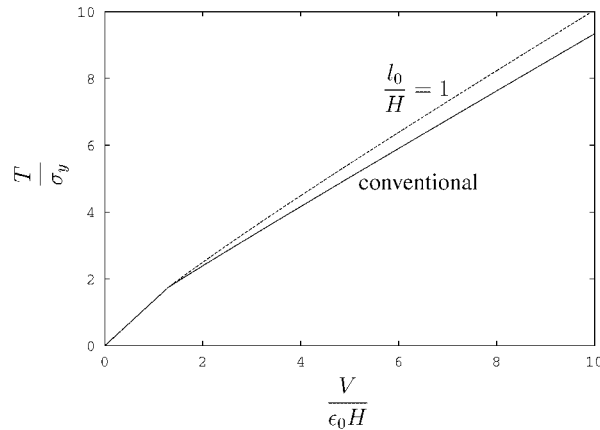


Figure 5. Tension responses for an infinite slab. The lower curve shows results for a conventional material, while the upper curve shows the response for a material with $l_0/H = 1$, and full constraint on the plastic flow at the platens.

The numerical results presented here for the shear problem, and also for the tension problem in the next section, are all performed using 10 quadrilaterals of aspect ratio one through the half thickness of the slab. For the gradient dependent analyses the results obtained do not change significantly when using more elements. On the other hand, conventional analyses with inhomogeneous stress states tend to be more sensitive to mesh refinement within the present numerical framework, and somewhat softer responses would be predicted for these problems, when using more refined meshes.

5.2. Normal separation of a finite slab

Rigid platens attached to the same rectangular slab considered in the previous section are now subject to normal separation, i.e. $u_1 = 0$, $u_2 = V$ on $x_2 = H$ and $u_1 = 0$, $u_2 = -V$ on $x_2 = -H$. The material parameters governing the stress–strain curve are the same as those used in the shear analysis.

The infinite slab experiences deformation that is independent of position with uniaxial straining at each point, and hence gradient effects can only arise as result of constraint of plastic flow at the platens. The plastic strain has $\dot{\epsilon}_{11}^p = \dot{\epsilon}_{33}^p = -\dot{\epsilon}_{22}^p/2$. The lateral plastic strain components are necessarily accompanied by offsetting elastic strains such that $\dot{\epsilon}_{11} = \dot{\epsilon}_{33} = 0$. As a consequence, the slope of the traction–separation relation, $T = \sigma_{22}$ versus V/H , scales with the elastic modulus in the plastic range and a large mean stress develops. Two traction–separation curves for the infinite slab are plotted in Figure 5, one for the conventional solid and the other for the multi-parameter strain gradient solid with $l_0 = \sqrt{\frac{9}{10} l_1^2 + \frac{8}{5} l_3^2}$ and $\dot{\epsilon}^p = 0$ imposed at the interface with the rigid platens. For the infinite slab in uniaxial straining, l_2 has no influence and the other parameters combine to give l_0 . The single parameter version gives identical predictions with $l_* = l_0$. The effect of the strain gradients on hardening is relatively small because the slope is dominated by the accompanying elastic strains. If the plastic strain was unconstrained at the platen interface there would be no difference between

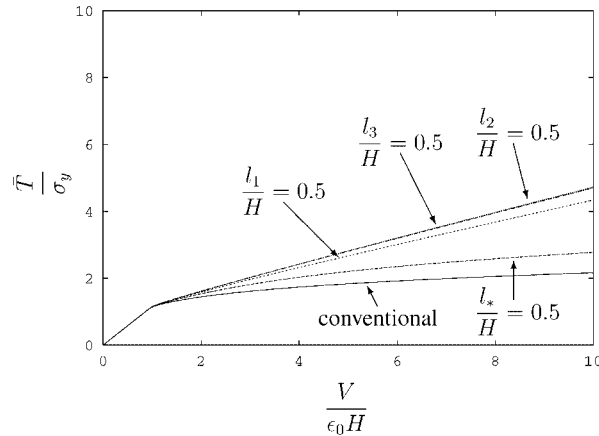


Figure 6. Tension responses for a slab of aspect ratio $L/H = 1$ with full constraint on plastic flow at the platens. For each of the upper 4 curves one of the length parameter is put equal to $H/2$, with all other length parameters put equal to zero. The lower curve shows the response for a conventional solid.

the conventional solid and the strain gradient solid because the conventional problem has no strain gradients.

The large mean stress is relaxed in the vicinity of the free ends, and a square slab experiences much larger separation at a given average normal traction, \bar{T} , than is the case for the infinite slab, as can be seen in Figure 6. In this plot, the four curves for the strain gradient solids are all computed with $\bar{\epsilon}^p = 0$ imposed at the interface with the rigid platens. The conventional result is also included, which now has non-zero strain gradients due to the effect of the traction-free ends. The single parameter version for a length parameter, $l_*/H = 0.5$, produces considerably less hardening amplification than the multi-parameter versions with length scales of the same magnitude. This difference is attributed to the same restricted dependence on the gradients of plastic strain discussed in connection with the shear problem. Note that even though l_2 gives rise to no extra hardening for the infinite slab, it nevertheless has almost an identical effect on hardening as l_3 for the square slab.

Results for two aspect ratios are shown in Figure 7 for the conventional solid and for the multi-parameter gradient solid with $l_1/H = l_2/H = l_3/H = \frac{1}{2}$. In addition, the effect of constraining plastic flow at the platens versus unconstrained flow is also presented. As expected, the larger aspect ratio slab has a significantly higher traction–separation curve due to the build up of mean stress in the central section of the slab. Nevertheless, both slabs display a strong influence of gradient effects on the apparent hardening. On the other hand, for this deformation the effect of constraint on the plastic flow, versus no constraint, is relatively small.

5.3. Indentation by a flat punch

Plane strain indentation by a rigid flat punch into a rectangular elastic-plastic solid is considered. The in-plane dimensions of the body are $2H \times H$ (Figure 8), the punch force per unit depth is P , and the width of the punch is $2c$. The conditions along the boundary of the slab and a rigid substrate (S_s) are that the displacements vanish with no constraint on plastic

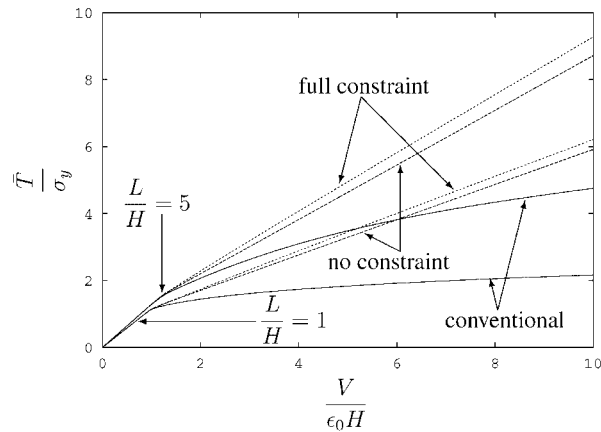


Figure 7. Tension responses for slabs of aspect ratios of 1 and 5. One set of curves show results for a gradient dependent material with full constraint on plastic flow at the platens, while the other set of curves show results for a gradient dependent material with no constraint on plastic flow at the platens. The material length scales are defined by $l_1/H = l_2/H = l_3/H = \frac{1}{2}$. The third set of curves show the conventional responses.

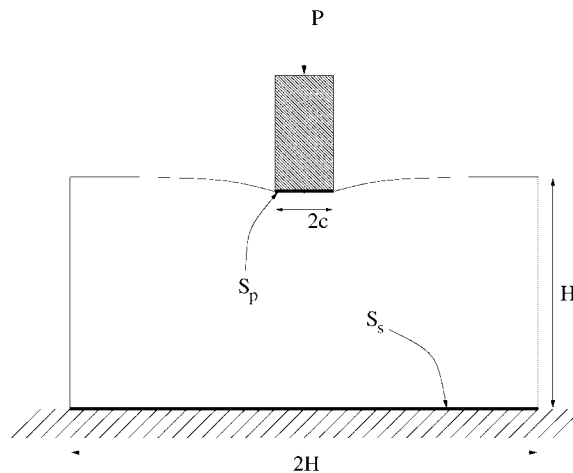


Figure 8. Indentation of a rigid rectangular indenter into an elastic-plastic solid on a rigid substrate is considered.

flow such that the higher order traction vanishes. Along the interface between the punch and the slab (S_p), the vertical displacement increment, $\dot{u}_2 = \dot{V}$, is prescribed with $\dot{u}_1 = 0$ and no constraint on plastic flow. Selected results have been obtained with plastic flow constrained to be zero on S_p , as will be discussed below. The material is again characterized by $\sigma_y/E = 0.01$, $\nu = 0.3$ and $n = 5$. In the numerical examples, $c/H = 0.1$.

Figure 9 displays the indentation curves in the form of $P/(2c\sigma_y)$ as a function of $V/(\epsilon_0 c)$ for the conventional solid and for solids with several choices of length parameters. It is

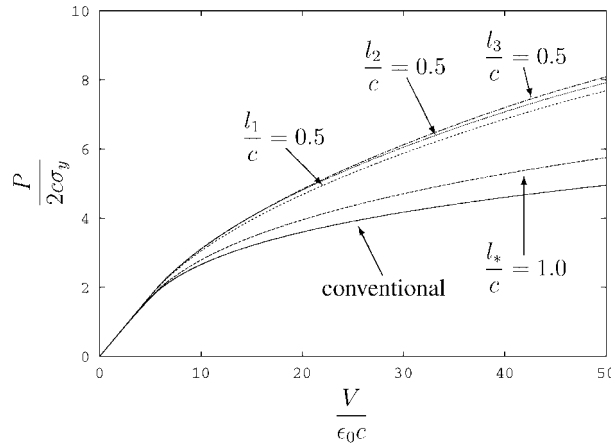


Figure 9. Punch responses for conventional and gradient dependent material behaviour. For each of the upper 3 curves one of the length parameters in the multi-parameter theory is put equal to $c/2$, with all other length parameters put equal to zero. The lower curves show the responses for a conventional solid, and for a gradient dependent material with $l_*/c = 1$.

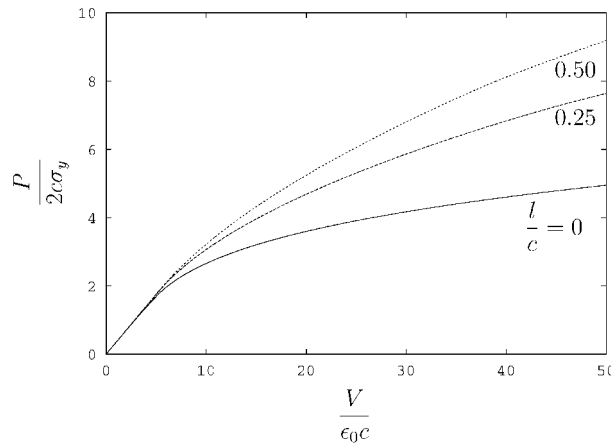


Figure 10. Punch response for different values of $l = l_1 = l_2 = l_3$.

evident that for this problem each of the length parameters in the multi-parameter version has essentially the same influence as the others. The apparent hardening when $l_1/c = \frac{1}{2}$ (or $l_2/c = \frac{1}{2}$, or $l_3/c = \frac{1}{2}$) is appreciable. Apparent hardening predicted by the single parameter version is comparatively much less, even when its length parameter l_* is doubled. The effect of the length parameters acting in combination, $l = l_1 = l_2 = l_3$, is shown in Figure 10. Associated contours of the effective plastic strain, ϵ^p , for both the conventional problem and for the multi-parameter version with $l/c = \frac{1}{2}$ are shown in Figure 11, in each case at the same indentation displacement, $V/(\epsilon_0 c)$. The larger force required to produce the indentation in the strain gradient solid gives rise to a larger plastic zone. At the same time, the plastic strain gradients are diminished in

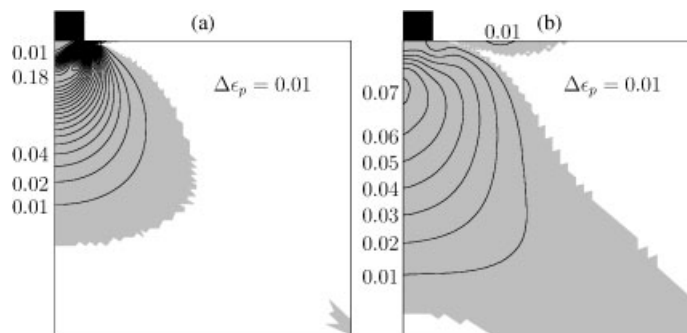


Figure 11. Contours of effective plastic strain, ϵ_p , for a punch indentation given by $V/(c\epsilon_0) = 50$: (a) Shows results for a conventional solid; and (b) shows the results for a strain gradient dependent solid with $l_1/c = l_2/c = l_3/c = \frac{1}{2}$. The shaded areas show the plastic zones.

the strain gradient solid. Generally, gradient hardening tends to smooth out gradients in plastic strain by hardening material in regions of high gradients relative to that in regions where the gradients are not so large.

Finally, the above results have been recalculated with two other boundary conditions under the punch: (i) frictionless interface ($\sigma_{12} = 0$) and (ii) full constraint on plastic flow ($\epsilon^p = 0$). These alternative conditions resulted in very small changes in the indentation curves. Thus, for indentation the issue of constraint of plastic flow under the indenter appears to be inconsequential. The 'natural' gradients dominate the size dependent hardening.

6. CONCLUDING REMARKS

The basic plane strain problems studied in this paper reveal several aspects of size effects for micron scale solid objects expected on the basis of strain gradient plasticity theory. Previous work has established that the material length parameters introduced in the theory when fit to experimental test data typically lie in the range from roughly one half a micron to two microns. Given the results presented here for the deformation of rectangular slabs by shear, normal tension and punch loads, one should expect size-dependent behaviour to set in when the smallest slab dimension (or the size of the punch) is on the order of roughly ten microns or smaller. The examples have brought out the importance of blockage of plastic flow at the boundary separating elastic and plastic regions. The constraint due to blockage of slip or dislocation motion cannot be modelled within the context of conventional plasticity theory. In problems where conventional theory predicts no gradients in plastic strain, the constraint on plastic flow will generally give rise to gradients and a resulting size effect. In some problems such as the punch problem or the slab with a low aspect ratio, the 'natural' gradients already give rise to a significant size effect and the effect of constraint on plastic flow plays a relatively less important role.

The formulation of the strain gradient theory employed here takes the effective plastic strain as one of the unknown field quantities and essentially treats it on a footing similar to the displacement components in the numerical analysis. The advantages of this formulation for numerical work were laid out by Reference [13–16]. For the most part, the present numerical

scheme has followed that presented by these authors. One issue that needs further attention is the physically correct continuity, or jump, conditions at the boundary between a plastic deforming region advancing into an elastic region. Here, we have argued that there should be no constraint on the increment of the amplitude of plastic strain on the loading side of the boundary on the physical grounds that dislocation motion, or slip, is not constrained there. This suggests that the solution must allow for a jump in the increment of plastic strain across an elastic-plastic boundary. More attention to the physical basis as well as the numerical representation may be called for.

The numerical examples bring out the difference between the multi-parameter version of the theory that involves the full tensor of the gradients of plastic strain and the single parameter version that is based solely on $\dot{\varepsilon}_i^p$. The examples illustrate that quantitative details of the size effect depend rather strongly on the theory invoked. Based on experimental data that is currently available, Fleck and Hutchinson [12] have argued that the multi-parameter version must be used if the theory is expected to be applicable to a wide range of phenomena embracing both stretch and shearing-type gradients. The present examples reinforce this finding in the sense that here it is observed that in some problems the two versions give quite comparable predictions, while in others they are quantitatively different.

REFERENCES

1. Stelmashenko NA, Walls MG, Brown LM, Milman YuV. Microindentations on W and Mo oriented single crystals: an STM study. *Acta Metallurgica et Materialia* 1993; **41**(10):2855–2865.
2. Stölken JS, Evans AG. A microbend test method for measuring the plasticity length scale. *Acta Materialia* 1998; **46**(14):5109–5115.
3. Fleck NA, Muller GM, Ashby MF, Hutchinson JW. Strain gradient plasticity: theory and experiment. *Acta Metallurgica et Materialia* 1994; **42**(2):475–488.
4. Kraft O, Hommel M, Arzt E. X-ray diffraction as a tool to study the mechanical behaviour of thin films. *Materials Science and Engineering A* 2000; **288**(2):209–216.
5. Arsenlis A, Parks DM. Crystallographic aspects of geometrically-necessary and statistically-stored dislocation density. *Acta Materialia* 1999; **47**(5):1597–1611.
6. Acharya A, Bassani JL. Lattice incompatibility and a gradient theory of crystal plasticity. *Journal of the Mechanics and Physics of Solids* 2000; **48**(8):1565–1595.
7. Gurtin ME. On the plasticity of single crystals: free energy, microforces, plastic-strain gradients. *Journal of the Mechanics and Physics of Solids* 2000; **48**(8):989–1036.
8. Fleck NA, Hutchinson JW. Strain Gradient Plasticity. *Advances in Applied Mechanics*, vol. 33, Academic Press: London, 1997; 295–361.
9. Gao H, Huang Y, Nix WD, Hutchinson JW. Mechanism-based strain gradient plasticity-I. Theory. *Journal of the Mechanics and Physics of Solids* 1999; **47**:1239–1263.
10. Acharya A, Bassani JL. On non-local flow theories that preserve the classical structure of incremental boundary value problems. In *IUTAM Symposium on Micromechanics of Plasticity and Damage of Multiphase Materials*. Pineau A, Zaoui A (eds), Kluwer Academic Publishers: Dordrecht, 1996; 3–9.
11. Aifantis EC. On the microstructural origin of certain inelastic models. *Transactions of the ASME. Journal of Engineering Materials and Technology* 1984; **106**(4):326–330.
12. Fleck NA, Hutchinson JW. A reformulation of strain gradient plasticity. *Journal of the Mechanics and Physics of Solids* 2001; **49**:2245–2271.
13. de Borst R, Mühlhaus H-B. Gradient-dependent plasticity: formulation and algorithmic aspects. *International Journal for Numerical Methods in Engineering* 1992; **35**:521–539.
14. de Borst R, Pamin J. Some novel developments in finite element procedures for gradient-dependent plasticity. *International Journal for Numerical Methods in Engineering* 1996; **39**:2477–2505.
15. Vardoulakis I, Aifantis EC. A gradient flow theory of plasticity for granular materials. *Acta Mechanica* 1991; **87**(3–4):197–217.
16. Mühlhaus H-B, Aifantis EC. A variational principle for gradient plasticity. *International Journal of Solids and Structures* 1991; **28**(7):845–857.